Cylindrical active coated nano-particles excited by electric and magnetic line sources

S. Arslanagic*, Y. Liu*, R. Malureanu+, R. W. Ziolkowski#

*Department of Electrical Engineering, Electromagnetic Systems, Technical University of Denmark
Ørsteds Plads, Bldg. 348, DK-2800 Kgs. Lyngby, Denmark
sar@elektro.dtu.dk

+ Department of Photonics Engineering, Technical University of Denmark
Ørsteds Plads, Bldg. 343, DK-2800 Kgs. Lyngby, Denmark

#Department of Electrical and Computer Engineering, University of Arizona
1230 E. Speedway Blvd. Tucson, Arizona, 85721-0104

***Abstract*—Cylindrical active coated nano-particles comprised of a silica nano-cylinder core covered with a plasmonic nano-shell are investigated with regard to their near- and far-field properties. The source of excitation is taken to be an electric or a magnetic line current, while three different plasmonic materials are employed for the nano-shells, namely silver, gold and copper.**

I. INTRODUCTION

Considerable efforts have been devoted to the field of metamaterials during the past decade. The regions of interest encompass microwave [1], as well as optical applications [2]. As to the optical domain, among the vast amount of discoveries, notable attention has been devoted to the design of metamaterials and their applications which incorporate active media with plasmonic materials [3], [4]. In particular it was shown that a properly designed active coated nano-particle (CNP) can lead to novel resonance and transparency effects as the intrinsic losses inherent to the plasmonic materials are overcome by suitable gain impregnation of the CNPs. In the majority of the studies of the above effects, the CNPs were taken to have a spherical shape; this was likewise most often the case in many of the previous studies of small particles with gain [5], [6].

While the properties of the passive coated cylindrical particles in the presence of an arbitrarily located electric line source (ELS) were thoroughly examined in [7], the present work reports the extension of these studies to the corresponding configurations employing active cylindrical CNPs. The nano-particles are made of specific dielectric materials, while silver, gold and copper are employed as plasmonic materials to investigate the amount of gain needed to overcome the loss in the different cases. The gain model employed in the entire analysis is the canonical, single frequency model, and values of the optical gain constant are used for different plasmonic materials. The analysis of the cylindrical active CNPs is conducted with a thorough investigation of their near- and far-field properties for altering locations of the ELS. Throughout the work, the time factor $\exp(j\omega t)$, with ω being the angular frequency and t being the time, is assumed and suppressed.

II. CONFIGURATION

The CNP configuration is depicted in Figure 1. It consists of a nano-cylinder (region 1) with radius ρ_1, covered with a concentric cylindrical nano-shell (region 2) with outer radius ρ_2. The host medium (region 3) of the CNP is that of free-space with the permittivity, ε_0, permeability, μ_0, and wave number, $k_0 = \omega\sqrt{\varepsilon_0\mu_0} = 2\pi/\lambda$, where λ is the wavelength. The CNP is excited by an arbitrarily located line source for which two polarizations are considered: the TM (with respect to z) polarization, in which case the source is an electric line source (ELS) with constant electric current I_e [A/m], and the TE (with respect to z) polarization, in which case the source is a magnetic line source (MLS) with constant magnetic current I_m [V/m]. The two regions 1 and 2 consist of simple and lossy materials with the permittivity, $\varepsilon_i = \varepsilon_i' - j\varepsilon_i''$, permeability, $\mu_i = \mu_0$, and wave number $k_i = \omega\sqrt{\varepsilon_i\mu_0}$, i=1 and 2, where the branch of the square root will be discussed below.

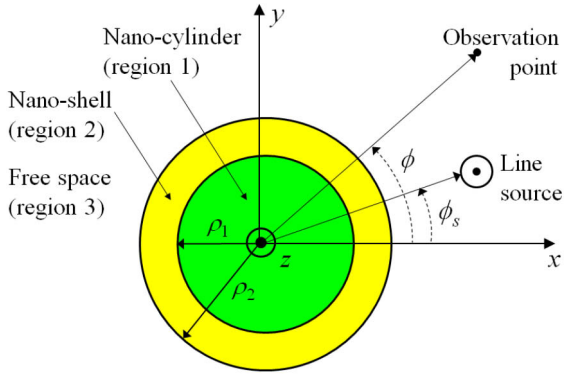

Fig. 1 The configuration of a CNP excited by a line source.

A cylindrical coordinate system (ρ, ϕ, z) and the associated rectangular coordinate system (x, y, z) are

introduced such that the origin of these coincide with the center of the CNP. The coordinates of the observation point are (ρ,ϕ), and those of the EHD are (ρ_s,ϕ_s).

III. THEORY

The analytical solution to the problem depicted in Figure 1 is rather straightforward to obtain and it has been outlined in detail in [7]. For the purpose of the present work we only present its main points.

For both polarizations, the field due to the line source constitutes the known incident field and it is expanded in terms of cylindrical wave functions. The unknown fields due to the CNP in the three regions are likewise expanded in terms of cylindrical wave functions and they involve the unknown expansion coefficients $C_{i,n}^{TM}$ for TM polarization, and $C_{i,n}^{TE}$ for TE polarization. For both sets of coefficients, $i=1$ for the field in region 1, $i=2$ and 3 for the field in region 2, and $i=4$ for the field in region 3, while the symbol n is the mode number with $n=0$ referring to the monopole mode in the expansion, $n=1$ to the dipole mode, etc. for the other modes. The unknown expansion coefficients depend on the location of the line source, and are easily obtained by enforcing the boundary conditions on the two spherical interfaces, $r=r_1$ and $r=r_2$.

For the purposes of our investigations of the electromagnetic properties of the CNP excited by the respective line sources, the normalized radiation resistance (NRR) is examined along with the spatial distribution of the electric and magnetic fields. The NRR is the ratio of the radiation resistance, R_t, of the line source in the presence of the CNP to its radiation resistance, R_i, in the absence of the CNP. In mathematical terms, the NRR is given by

$$\text{NRR} \equiv \frac{R_t}{R_i} = \frac{1}{2}\sum_{n=0}^{N_{\max}} \tau_n^2 (3-\tau_n) |\alpha_n|^2 , \qquad (1)$$

where

$$\alpha_n = \begin{cases} C_{4,n}^{TM} & \text{ELS in region 1 and 2} \\ J_n(k_0\rho_s) + C_{4,n}^{TM} & \text{ELS in region 3} \end{cases} \qquad (2a)$$

for TM polarization, and

$$\alpha_n = \begin{cases} C_{4,n}^{TE} & \text{MLS in region 1 and 2} \\ J_n(k_0\rho_s) + C_{4,n}^{TE} & \text{MLS in region 3} \end{cases} \qquad (2b)$$

for TE polarization. In (1) and (2), $J_n(k_0\rho_s)$ is the Bessel function of order n, τ_n is the Neumann number, i.e., $\tau_n=1$ for $n=0$ mode and $\tau_n=2$ otherwise, while $N_{\max}$ is the truncation limit in the implementation of the exact infinite summation and is chosen to ensure the convergence of the expansion in (1).

IV. GAIN AND MATERIAL MODELS

The present work examines three different CNPs. For each of them, region 1 is composed of silica (SiO_2) nano-cylinder core, while three different plasmonic materials are considered for the nano-shell of region 2: silver (Ag), gold (Au) and Copper (Cu). The corresponding structures are referred to as the Ag-, Au-, and Cu-based cylindrical CNPs. The radius of the nano-cylinder is for all CNPs set to $r_1=24\,\text{nm}$ while the outer radius of the nano-shell is $r_2=30\,\text{nm}$, resulting in a 6 nm thick plasmonic nano-shell. This choice matches the spherical active CNP cases considered in [3] and [4].

The permittivity, ε_1, of the silica nano-sphere is comprised from a contribution from its refractive index in the frequency region of interest ($n=\sqrt{2.05}$) and a contribution from the canonical gain model and is thus expressed as

$$\varepsilon_1 = \varepsilon_0 (n^2 - \kappa^2 - j2n\kappa) , \qquad (3)$$

where κ determines the nature of the nano-cylinder which is lossless and passive for $\kappa=0$, lossy and passive for $\kappa>0$, and active for $\kappa<0$. Thus the amount of gain introduced in the CNP configuration to overcome the plasmonic material losses is tailored by the choice of the parameter κ.

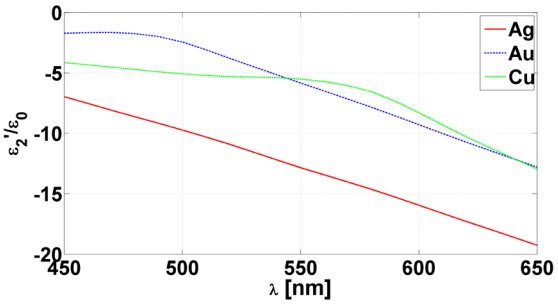

(a)

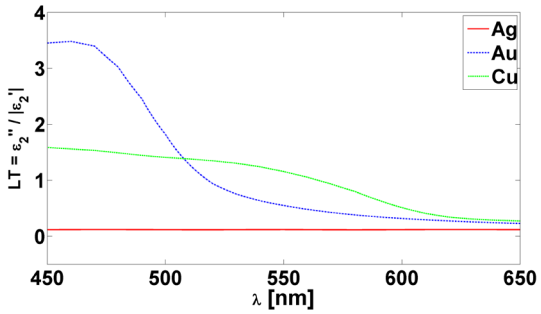

(b)

Fig. 2 (a) The real, ε_2', part of the 6 nm thick Au, Ag, and Cu nano-shells normalized to the free-space permittivity ε_0, and (b) the corresponding loss tangents $\text{LT} = \varepsilon_2'' / |\varepsilon_2'|$.

As to the permittivity, ε_2, of the plasmonic nano-shell we note that its size dependency must be taken into account due to the nano-scale dimension of the CNPs. To this end,

empirically determined bulk values of Ag, Au and Cu permittivities have been employed [1] and their real parts, ε_2', normalized with the free-space permittivity ε_0, are shown in Figure 2 for a 6 nm thick Ag, Au, and Cu nano-shell along with the associated values of their loss tangents defined by $\mathrm{LT} = \varepsilon_2'' / |\varepsilon_2'|$ as functions of the excitation wavelength.

As observed in Figure 2, the real part of the permittivity of the various plasmonic materials under consideration is negative in the depicted wavelength range, and moreover that they all are lossy with Ag being the least lossy case.

V. NUMERICAL RESULTS

First, the results pertaining to the TM polarization are shown and discussed, and are followed by those for the TE polarization. The currents of the corresponding sources are set to $I_e = 1$ [A/m] and $I_m = 1$ [V/m], respectively.

A. TM polarization

Figure 3 shows the NRR as a function of the wavelength, λ, for the Ag-based CNP for different values of the parameter κ. The ELS is located in region 1 at $(\rho_s, \phi_s) = (12\,\mathrm{nm}, 0^o)$.

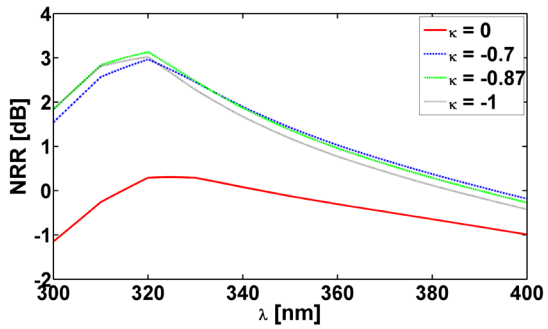

Fig. 3 The NRR as a function of the wavelength, λ, of the Ag-based CNPs for different values of parameter κ. The ELS is in region 1 at $(\rho_s, \phi_s) = (12\,\mathrm{nm}, 0^o)$.

It is rather obvious that for this particular polarization, no resonance, i.e., large values of the NRR, is in evidence, regardless of the value of κ. The quantity NRR ≈ 0.3dB for $\kappa = 0$ at $\lambda = 324.6$ nm, while NRR ≈ 3.13dB for $\kappa = -0.87$ at $\lambda = 320$ nm. This is an expected result since the resonance condition [7], [8]

$$\frac{\rho_1}{\rho_2} \approx 2n\sqrt{\frac{(\mu_2' + \mu_1')(\mu_2' + \mu_0)}{(\mu_2' - \mu_1')(\mu_2' - \mu_0)}}, \quad n \geq 1 \qquad (4)$$

holds for the corresponding small lossless structure of Fig. 1 in the case of TM polarization. As shown in [7] and [8], at least one of the parameters, μ_1' or μ_2', must be negative to satisfy (4) and thus provide large NRR values. However, since for the CNP in question, as well as for the remaining two CNPs, the permeabilities of all regions are those of free-space, no resonance and, thus, no enhancement of the NRR occurs for this particular polarization. This is further illustrated with Fig. 4 which shows the quantity $20\log_{10}|\vec{E}(\rho,\phi)|$, where $\vec{E}(\rho,\phi)$ is the total electric field normalized by 1 V/m, in a circular region of radius 90 nm for the Ag-based CNP for $\kappa = 0$, $\lambda = 324.6$ nm (Fig. 4a) and $\kappa = -0.87$, $\lambda = 320$ nm (Fig. 4b). In both cases, the field is entirely that of the ELS alone, i.e., the CNP does not exhibit an influence on the ELS. Although not shown, similar results were found for the Au- and Cu-based CNPs.

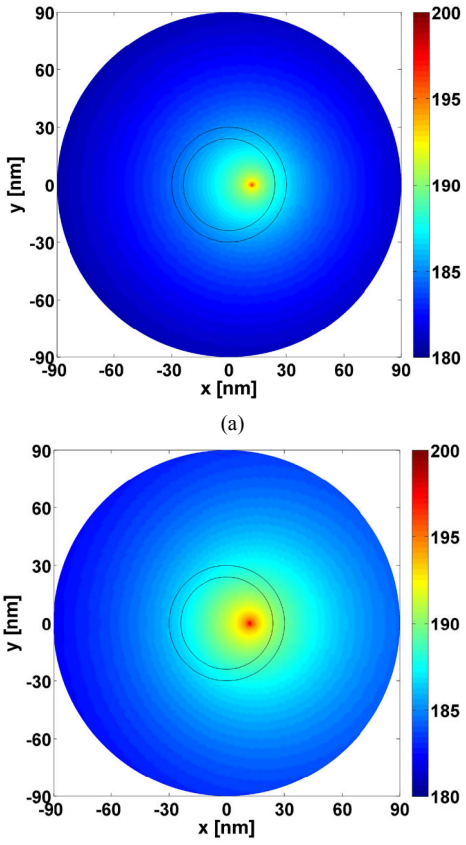

Fig. 4 Electric field of the Ag-based CNP for (a) $\kappa = 0$, $\lambda = 324.6$ nm, and (b) $\kappa = -0.87$, $\lambda = 320$ nm. The ELS is located in region 1 at $(\rho_s, \phi_s) = (12\,\mathrm{nm}, 0^o)$. The curves representing the cylindrical surfaces of the CNP are shown in the figure.

B. TE polarization

Figure 5 shows the NRR as a function of the wavelength, λ, for the three CNPs with (a) $\kappa = 0$ and (b) the corresponding super-resonant states which occur with $\kappa = -0.175$, $\kappa = -0.262$ and $\kappa = -0.310$, respectively, for the Ag-, Au-, and Cu-based CNPs. In all cases, the MLS is in

region 1 at $(\rho_s, \phi_s) = (12\,\text{nm}, 0^o)$. For the super-resonant states the NRR values are significantly increased and the intrinsic losses of the plasmonic materials are significantly overcome relative to the lossless-core and passive CNP results reported in Fig. 5(a). The NRR values, as well as the values of the parameter κ needed for the super-resonance to occur, are summarized in Table 1 for the three CNPs along with the values of the wavelength λ at which the respective resonances are attained.

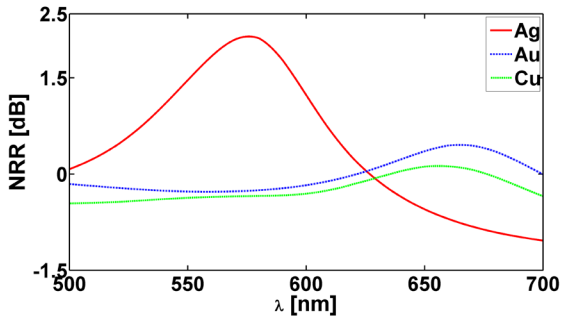

(a) Lossless-core CNPs.

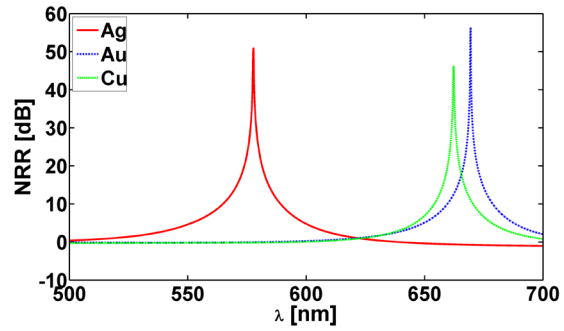

(b) Super-resonant CNPs.

Fig. 5 The NRR as a function of the wavelength, λ, of the lossless core (a) and super-resonant (b) Ag-, Au-, and Cu-based CNPs. The MLS is in region 1 at $(\rho_s, \phi_s) = (12\,\text{nm}, 0^o)$.

TABLE I

THE VALUES OF NRR, PARAMETER κ, AND WAVELENGTH λ FOR THE SUPER-RESONANT STATES FOR THE AG-, AU-, AND CU-BASED CNPS WHEN THE MLS IS IN REGION 1 AT $(\rho_s, \phi_s) = (12\,\text{nm}, 0^o)$

Parameter	Ag	Au	Cu
NRR [dB]	51.06	56.39	46.26
κ	-0.175	-0.262	-0.310
λ [nm]	577.70	669.39	662.19

The super-resonances reported in Fig. 5(a) are due to a strong excitation of the dipole mode in the respective CNPs. This is confirmed in Fig. 6(b) which shows the spatial distribution of the total magnetic field (more specifically, the quantity $20\log_{10}|\vec{H}(\rho,\phi)|$), where $\vec{H}(\rho,\phi)$ is the total magnetic field normalized by 1 A/m, for the Ag-based CNP with $\kappa = -0.175$ and $\lambda = 577.70\,\text{nm}$, where a clear and strong dipolar field distribution is in evidence. In contrast, the magnetic field of the corresponding lossless and passive Ag-based CNP ($\kappa = 0$) reported in Fig. 6(a) is a mixture of monopole and dipole modes this being insufficient to provide enhancement of the NRR. These results are in agreement with the results of Fig. 5.

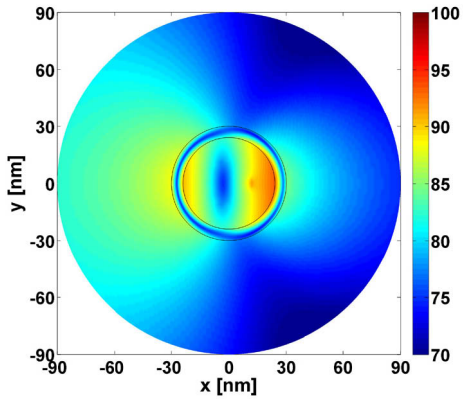

(a)

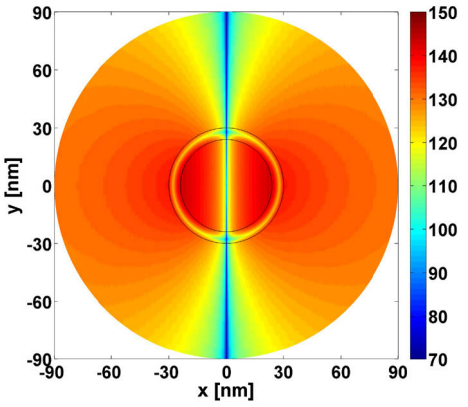

(b)

Fig. 6 Magnetic field of the Ag-based CNP for (a) $\kappa = 0$, $\lambda = 575.69\,\text{nm}$, and (b) $\kappa = -0.175$, $\lambda = 577.70\,\text{nm}$. The MLS is located in region 1 at $(\rho_s, \phi_s) = (12\,\text{nm}, 0^o)$. Note that the dynamic range in (b) is larger than in (a). The curves representing the cylindrical surfaces of the CNP are shown in the figure.

Although not shown, the magnetic field distribution for the Au- and Cu-based CNPs in their super-resonant states resembles that of the Ag-based CNP, i.e., the large NRR values for these CNPs are likewise due to the excitation of the resonant dipole mode inside the CNPs. It is interesting to remark that these results are in line with the resonance condition [7], [8]

$$\frac{\rho_1}{\rho_2} \approx \sqrt[2n]{\frac{(\varepsilon_2' + \varepsilon_1')(\varepsilon_2' + \varepsilon_0)}{(\varepsilon_2' - \varepsilon_1')(\varepsilon_2' - \varepsilon_0)}}, \quad n \geq 1 \tag{5}$$

which holds for the corresponding small lossless structure of Fig. 1 in the case of TE polarization. As shown in [7] and [8], at least one of the parameters, ε_1' or ε_2', must be negative to satisfy (4) and thus provide large NRR values. This requirement can be fulfilled here due to the negative values of ε_2' of the employed plasmonic materials, cf., Fig. 2(a).

The resonant behavior of the three examined CNPs is not restricted to the MLS in region 1, but also occurs when it is in region 2 and 3 as shown in Fig. 7, where the NRR is given as a function of the MLS location, ρ_s, for the three super-resonant CNPs. With no enhancements when the MLS is at and very close to the origin, rather large values of the NRR result when it is close to the inner surface of the plasmonic shells. Moreover, a dip in the NRR is noted in region 2 for all cases; at these locations the excited resonant dipole mode is somewhat weaker than that shown in Fig. 6(b). This is illustrated by Fig. 8 where the magnetic field is shown for the MLS location ($\rho_s = 27.84$ nm) of the minimum NRR in region 2 for the super-resonant Ag-based CNP.

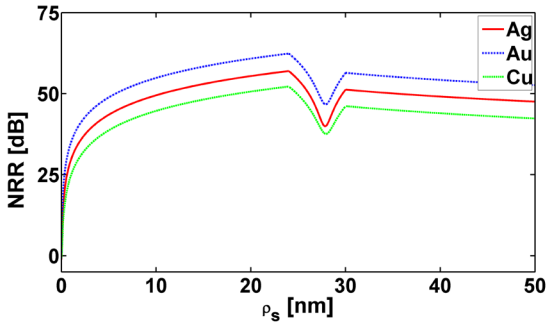

Fig. 7 The NRR as a function of the MLS location, ρ_s, of the super-resonant Ag-, Au-, and Cu-based CNPs.

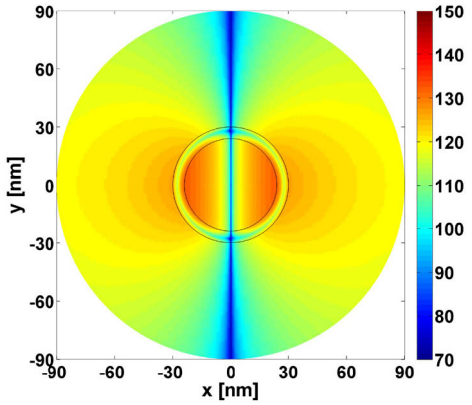

Fig. 8 Magnetic field of the Ag-based CNP for $\kappa = -0.175$, $\lambda = 577.70$ nm. The MLS is located in region 2 at $(\rho_s, \phi_s) = (27.84\text{ nm}, 0^o)$, this being the location at which the minimum NRR is attained in Fig. 7. The curves representing the cylindrical surfaces of the CNP are shown in the figure.

VI. SUMMARY AND CONCLUSIONS

Electromagnetic properties of infinitely long cylindrical coated nano-particle configurations comprised of a silica nano-cylinder core covered with a plasmonic nano-shell were investigated in the present work. The source of excitation was taken to be an electric or a magnetic line current, while three different plasmonic materials were employed for the nano-shells, namely silver, gold and copper.

While no resonant phenomenon was observed for the case of the electric line source illumination, for the passive as well as active configurations, it was demonstrated that the inclusion of gain in the silica nano-cylinder significantly helps to overcome the intrinsic losses of the plasmonic nano-shells for the case of magnetic line source illumination. In particular, super-resonant states were identified for the silver-, gold-, and copper-based coated nano-particles and their large enhancements of the normalized radiation resistance were quantified. These enhancements were shown to be due to a strong excitation of the dipole mode inside the respective particles, and were largest for the source locations near-by the inner surface of the nano-shells, while being heavily diminished for source locations near to the center of the particles, in agreement with similar findings for the purely passive cases [7]. The amount of gain required in the three cases was different and was found, as expected, to be largest for the most lossy material. The existence of the super-resonances for the case of the magnetic line source illumination and their absence for the electric line source case was found to be in agreement with the predictions of certain conditions for resonances derived in literature for metamaterial-based structures.

REFERENCES

[1] N. Engheta and R. W. Ziolkowski, (Eds.), *Metamaterials: Physics and Engineering Explorations*, (IEEE Press, Wiley Publishing), 2006.

[2] V.M. Shalaev, "Optical negative-index metamaterials" *Nature Photon* **1** 41-48, 2007.

[3] J. A. Gordon and R. W. Ziolkowski, "Investigating functionalized active coated nano-particles for use in nano-sensing applications," *Opt. Exp.*, vol. 15, 12562-12582, Oct. 2007.

[4] J. A. Gordon and R. W. Ziolkowski, "Optical CNP metamaterials," *Opt. Exp.*, vol. 16, pp. 6692-6716, Apr. 2008.

[5] N. G. Alexopoulos and N. K. Uzungolu, "Electromangetic scattering from active objects: invisible scatters," *Appl. Opt.*, Vol. 17, 235-239, 1978.

[6] H. W. Chew, McNulty P. J., and M. Kerker, "Model for a Raman and fluorescent scattering by molecules embedded in small particles," *Phys. Rev. A*, vol. 13, 396-404, 1976.

[7] S. Arslanagic, R. W. Ziolkowski, and O. Breinbjerg, "Analytical and numerical investigation of the radiation and scattering from concentric metamaterial cylinders excited by an electric line source," *Radio Sci.*, vol. 42, RS6S15, doi: 10.1029/2007RS 003644, Nov. 2007.

[8] A. Alú and N. Engheta, "Resonances in sub-wavelength cylindrical structures made of pairs of double-negative and double-positive or epsilon-negative and mu-negative coaxial shells," ICEAA, Turin, Italy, Sept. 8-12, 2003, pp. 435-438.